Published in final edited form as:
Cancer Res. 2012 November 15; 72(22): 5921–5933. doi:10.1158/0008-5472.CAN-12-0736.

Temporal molecular and biological assessment of an erlotinib-resistant lung adenocarcinoma model reveals markers of tumor progression and treatment response

Zoë Weaver[1,*], **Simone Difilippantonio**[1,*], **Julian Carretero**[2,3,4,*], **Philip L. Martin**[1], **Rajaa El Meskini**[1], **Anthony J. Iacovelli**[1], **Michelle Gumprecht**[1], **Alan Kulaga**[1], **Theresa Guerin**[1], **Jerome Schlomer**[1], **Maureen Baran**[1], **Serguei Kozlov**[1], **Thomas McCann**[5], **Salvador Mena**[4], **Fatima Al-Shahrour**[6,7], **Danny Alexander**[8], **Kwok-Kin Wong**[2,3], and **Terry Van Dyke**[1,9]

[1]Center for Advanced Preclinical Research, SAIC-Frederick, Inc., Frederick National Laboratory for Cancer Research/NCI, Frederick, MD 21702

[2]Genetics Division, Department of Medicine Brigham and Women's Hospital, Harvard Medical School, Boston, MA 02115

[3]Ludwig Center at Dana-Farber/Harvard Cancer Center, Boston, MA 02115

[4]Department of Physiology, University of Valencia, Burjassot 46100, Spain

[5]Molecular Imaging Program, National Cancer Institute, NIH, Bethesda, MD 20892

[6]Division of Hematology, Department of Medicine, Brigham and Women's Hospital, Harvard Medical School, Boston, MA 02115

[7]Broad Institute of MIT and Harvard, Cambridge, MA 02142

[8]Metabolon, Inc., Durham, NC, 27713

[9]Mouse Cancer Genetics Program, Frederick National Laboratory for Cancer Research/NCI, 1050 Boyles St., Frederick, MD 21702

Abstract

Lung cancer patients with activating mutations in the epidermal growth factor receptor (EGFR) kinase who are treated long-term with tyrosine kinase inhibitors (TKIs) often develop secondary mutations in EGFR associated with resistance. Mice engineered to develop lung adenocarcinomas driven by the human EGFR T790M resistance mutation are similarly resistant to the EGFR TKI erlotinib. By tumor volume endpoint analysis, these mouse tumors respond to BIBW 2992 (an irreversible EGFR/HER2 TKI) and rapamycin combination therapy. In order to correlate EGFR-driven changes in the lung with response to drug treatment, we performed an integrative analysis of global transcriptome and metabolite profiling compared to quantitative imaging and histopathology at several time points during tumor progression and treatment. Responses to single drug treatments were temporary, while combination therapy elicited a sustained response. During tumor development, metabolomic signatures indicated a shift to high anabolic activity and suppression of anti-tumor programs with 11 metabolites consistently present in both lung tissue and blood. Combination drug treatment reversed many of the molecular changes found in tumored lung. Data integration linking cancer signaling networks with metabolic activity identified key

Corresponding Author: Terry Van Dyke, Mouse Cancer Genetics Program, Frederick National Laboratory for Cancer Research/NCI, 1050 Boyles St., Frederick, MD 21702 vandyket@mail.nih.gov; Phone: 301-846-1988.
*these authors contributed equally

Potential Conflicts of Interest: None of the authors have any conflict of interest.

pathways such as glutamine and glutathione metabolism that signified response to single or dual treatments. Results from combination drug treatment suggest that metabolic transcriptional control through C-MYC and SREBP, as well as ELK1, NRF1 and NRF2, depends on both EGFR and mTORC1 signaling. Our findings establish the importance of kinetic therapeutic studies in preclinical assessment and provide in vivo evidence that TKI-mediated antiproliferative effects also manifest in specific metabolic regulation.

Keywords

lung cancer; EGFR; mouse model; BIBW 2992; rapamycin

INTRODUCTION

Lung cancer is the leading cause of cancer-related deaths (1). Current screening methods for early disease are ineffective at improving the 5-year survival rate, which is < 4% for advanced non-small cell lung cancer (NSCLC)(2). For most cancers, including NSCLC, traditional cytotoxic chemotherapy has limited efficacy, and patients develop resistance to targeted inhibitors, indicating the need for identification of molecular networks operative in disease and treatment response. In particular, effective preclinical systems are required for guidance on patient stratification, therapeutic directives and response biomarkers. Such needs are exemplified by the current status of NSCLC clinical management. Activating mutations in EGFR, such as the L858R mutation, are effective predictors of response to EGFR TKI therapy (3). While most patients initially respond to EGFR TKIs, the majority relapse within 6-12 months, underscoring the importance of identifying therapies that overcome or mitigate such resistance. Strikingly, a single secondary missense mutation in the EGFR TK domain, T790M, is associated with >50% of acquired resistance cases (4).

Recent advances in the ability to globally assess molecular networks responsive to biological and chemical perturbations in cancer have facilitated unbiased discovery in disease mechanisms (5). Genetically engineered mouse (GEM) models can facilitate both assessment of disease etiology from initiation through progression as well as treatment responses within the organs/cells of interest (6). Mice engineered to develop erlotinib-resistant lung adenocarcinomas driven by human EGFR L858R;T790M mutations (EGFR-TL) (7, 8) respond to BIBW 2992 (afatinib, an irreversible EGFR/HER2 TKI currently in clinical trial) and rapamycin combination therapy, based on tumor volume endpoints (9). BIBW 2992 or rapamycin alone minimally inhibit tumor growth. To further assess responses to single and combination therapies, and to gain insight into the optimal strategy for preclinical evaluation in robust cancer models, we examined both transcriptional and metabolic profiles in disease induction and therapeutic response with time. These studies underscore the value of temporal well-powered evaluations and offer an opportunity to identify surrogate markers for disease and treatment responses and for tailoring therapeutic regimens.

MATERIALS AND METHODS

Tumor induction and sampling

Mice (see Supplementary Materials and Methods) were fed 200mg/kg doxycycline feed from Research Diets. Blood was taken from the mandibular vein of bitransgenic EGFR-L858R-T790M;CCSP-rtTA mice (E+R+) or mice carrying the CCSP-rtTA driver, but not the EGFR transgene (E-R+) at 2 weeks (n=6 for both E-R+ and E+R+) and when tumor growth required euthanasia of the mice (terminal at 6 to 8 weeks; n=8 for both E+R+ and E-R+), and snap-frozen in an equal volume of 9 mM EDTA in PBS. Lung tissue was harvested

and snap-frozen at 2 weeks and terminal stages, and age-matched control mice were taken at the same time points post-induction (pi). For treatment studies, blood and lung tissue were harvested after 1 (n=19), 2 (n=19), or 4 (n=40) weeks of daily treatment with drug vehicle, BIBW 2992 (20 mg/kg/day, oral gavage), rapamycin (2 mg/kg/day, i.p.), or the combination of both compounds starting at 4 weeks pi.

Histology/Pathology

Mice were euthanized at the indicated times and right lungs were inflated with formalin and processed for immunohistopathological analysis. Immunohistochemistry experiments are described in the Supplementary Data. H&E slides of lungs from drug and vehicle-treated tumors were scored blindly by a board certified veterinary pathologist (PLM) according to a grading scheme that was developed for this study (see Supplementary Data for details). All tumors (4-10) of each experimental group (vehicle or drug-treated) were analyzed.

Automated image acquisition and quantification

Immunohistochemistry for Ki-67 was performed on lung sections from each mouse and slides were scanned using the Ariol image scanning and analysis system (Applied Imaging Corp., Santa Clara, California) at 20X. As the severity of lung disease was heterogeneous between lung lobes, the percentage of Ki-67 positive cells was quantified in the lung lobe that was most representative of the overall histopathological score. The Kisight image analysis module was used to count the total number of nuclei in the lung section as well as the total number of Ki-67 positive (Brown-DAB) nuclei and Ki-67 negative (Blue-hematoxylin) nuclei. For each lung lobe approximately 30,000 to 125,000 nuclei were counted.

Gene Expression Profiling

Preparation of RNA is described in the Supplementary Data. Hybridization to Mouse Gene 1.0 ST chips was performed following Affymetrix protocols (Affymetrix, Inc.). Hierarchical clustering analysis was performed using pairwise complete linkage method with the Pearson correlation distance measure employing the Genepattern genomic analysis platform.“Single Sample” Gene Set Enrichment Analysis (10, 11) was used to determine the degree of absolute enrichment of GO biological processes gene sets (12) in each sample within the gene expression data set. Signature values for each sample were normalized using the entire sample set. Standard GSEA was used to determine the enrichment of transcription factor binding sites between classes. Gene sets sharing a cis-regulatory motif that is conserved across the human, mouse, rat, and dog genomes (13), representing known or predicted regulatory elements in promoters and 3′-UTRs, were obtained from MSigDB (see Supplementary Data for details).

RESULTS

Temporal evaluation of tumor growth and treatment response reveals distinct dynamics of single vs. combination therapy

To examine responses elicited during human EGFR L858R-T790M-driven lung adenocarcinoma, as well as experimental treatment-induced regression, we measured changes with time in lung disease severity and tumor burden. Bitransgenic EGFR-L858R-T790M;CCSP-rtTA mice (designated E+R+) are engineered to develop lung adenocarcinoma upon EGFR transgene induction by doxycycline. Mice carrying the CCSP-rtTA driver, but not the EGFR transgene (E-R+) served as controls. E+R+ mice developed lung tumors when continuously exposed to doxycycline (doxy), and consistent with previous studies (7), adenomas were detectable by MRI and histology within 2-3 weeks pi,

progressing to adenocarcinomas that often involved entire lobes at terminal stages. Induced E+R+ mice were treated with BIBW 2992, rapamycin, or the combination daily for up to 4 weeks (Fig. 1A). In order to quantify histopathology response to drug treatment (or lack thereof) in the tumors, severity of disease was scored based on extent and morphology ranging from 0 (no lesions) to 5 (multifocal to coalescing adenocarcinoma) (Supplementary Data and Supplementary Fig. S1). The histopathological severity grade increased over time in the vehicle-treated group, and while each individual drug had some effect in suppressing tumor growth, the combination treatment was most effective (score of 1.9 compared to 4.3 for vehicle-treated after 4 weeks, $p = 0.002$) (Fig. 1B). Thus, the present expanded study agrees well with previous findings that used smaller cohorts (9). We also detected decreased cellular proliferation (by Ki-67 staining) and decrease in overall tumor burden (by H&E and confirmed by total EGFR staining) in both single and combination treatments. Combination treatment resulted in the greatest decrease in total EGFR, phospho-EGFR, and Ki-67 staining, even after only 1 week of treatment (Supplementary Fig. S2). Automated quantification of Ki-67 staining supports the hypothesis that the strongest effect on proliferation is from BIBW 2992 and rapamycin dual treatment at all time points (Fig. 1C), however, the Ki-67 data indicates an increase in proliferation after 4 weeks even in the combination-treated mice. Immunoblotting confirmed phospho-EGFR or phospho-S6 reduction in lungs of BIBW 2992 or rapamycin-treated mice (respectively) at 4, 8, and 24 hr post-single dose, as well as reduction of both in lungs of combination-treated mice (Supplementary Fig. S3). By 24 hr, reduction of phospho-EGFR was more variable, even in the combination-treated mice, indicating the need for continued treatment to achieve target suppression.

To attain another quantitative measure of treatment effects, baseline MRI measurements were compared with post-treatment tumor scans (Fig. 1D, E and Supplementary Data). In this model, signals on MRI reflect not only tumor burden, but also associated inflammation. After 1 week of treatment, BIBW 2992 alone resulted in tumor regression compared to baseline, whereas in the cohort treated for 2 weeks, tumor growth was inhibited by BIBW 2992 relative to vehicle, but regression was not observed. However, BIBW 2992 treatment together with rapamycin resulted in substantial tumor regression compared to baseline, evidenced by both 2 and 4 week post-treatment times.

Taken together, these results indicate that although BIBW 2992 successfully inhibits its primary target in vivo and elicits a short-term tumor regression response, it does not produce a sustained pathway and growth response unless combined with rapamycin. Importantly, maximal response for either single agent occurs early, with rebound apparent within a few weeks despite continous treatment. The kinetics of such responses are thus critical in evaluating therapeutic efficacy. During the course of treatment, some tumor regions responded to drug and thus overall tumor burden decreased, which is reflected in the MRI measurements (note that Fig. 1E is an example of the maximum regression response observed). However, as discussed above, at the histopathology level small areas of the affected lungs (below the resolution level of the MRI scan) were observed that were either refractory to treatment or developed resistance as detected by pathology score and Ki-67 data. Endpoint tumor size in this case measures the sum of treatment responses and emerging resistant growth, underscoring the importance of temporal assessment in preclinical models for accurate response measurements.

Gene expression reflects changes in oncogenic signaling in response to therapy over time

To further explore the mechanism(s) of synergy in combination treatment, lungs from control E-R+, tumor bearing E+R+ induced mice, and drug-treated E+R+ mice were analyzed for transcriptome changes. Gene expression data was subjected to supervised hiererarchical clustering to compare profiles of untreated tumor-bearing mice to drug-treated

for 1 or 4 weeks (Fig. 2A). As expected, vehicle-treated E+R+ samples had expression profiles similar to those of untreated E+R+ lung samples. The 1-week treated samples showed an almost universal suppression of gene expression compared to untreated or vehicle-treated E+R+ animals that did not distinguish between responders and non-responders by pathology score (Fig. 2A). However, after 4 weeks there were clearly several samples in which the profile more closely matched the normal gene expression profile (E-R + control). These lungs also had lower (less severe) pathology scores than the comparable vehicle-treated or untreated samples. Although most of the combination drug-treated tumors responded at the phenotypic level as seen by MRI scans and histopathology, not all of the samples appeared to be responders at the transcriptome level, indicating some heterogeneity within the tumors as discussed above. These data also point to the variability within treatments due to the mixed tumor cell population.

A single-sample Gene Set Enrichment Analysis (GSEA) of Gene Ontology (GO) terms was performed as a first step to reveal the biological functions that differentiate normal (E-R+) from tumor-bearing (E+R+) lung and vehicle- from drug-treated tumors. Among others, GO terms involved in cell metabolism, mitosis and DNA replication were differentially affected in EGFR tumors (Fig. 2B). We chose four genes in the signature (BUB1, TOP2A, CCNB2, and PLK1) for validation by qPCR (Supplementary Fig. S4). Of note, in a study of gene expression markers in human NSCLC, CCNB2 and TOP2A were part of a 187-gene signature set distinguishing normal tissues from malignant NSCLC (14). All four genes were downregulated after treatment with BIBW 2992 or rapamycin, and the drug combination caused a further decrease in gene expression levels. Fold-change levels compared to vehicle-treated controls were consistently greater after 1 week compared to 2 weeks of drug treatment, again indicating an greater early treatment response on average. The 4-week gene expression data was a more accurate indicator of which individual tumors exhibited a sustained response. We conclude that multiple time points during the course of treatment are crucial to profiling the in vivo activity of cancer drugs.

Tumor induction and drug response result in contrasting metabolomic alterations

To evaluate additional biological changes accompanying tumor induction and treatment that may correlate to gene expression responses, we performed metabolic profiling of blood and lung tissue from induced E-R+ and E+R+ mice at various time points and from E+R+ mice treated with the described drug regimen for 4 weeks. Using a high-throughput small-molecule analytical platform (Metabolon, Inc.; see Supplementary Materials and Methods), a total of 457 biochemicals were detected in lung, and 324 were detected in blood, including 238 compounds common to both lung and blood, 219 compounds unique to lung, and 86 compounds unique to blood (Supplementary Tables S1 and S2). Statistical comparisons were used to identify biochemicals whose relative levels differed between experimental groups (Supplementary Table S3 and Supplementary Materials and Methods). In lung tissue there were extensive metabolomic alterations consistent with tumor development within two weeks of induction of the EGFR transgene, which were typically stronger at the terminal time point (data summarized in Fig. 3A). These changes were characterized by a shift to high anabolic activity, including diversion of glucose oxidation to the pentose phosphate pathway, elevated amino acid and nucleotide pools, higher levels of polyamines, glycerolipids, and long-chain fatty acids.

Lipid pathway metabolites were upregulated as a result of tumor induction, including fatty acids (utilized in cell membrane construction, energy metabolism, and as substrates for signaling molecules), and phospholipids (essential for membrane biosynthesis) (Fig. 3A). For example, CDP-choline and intermediates to CDP-choline synthesis (choline and choline-phosphate) were increased in tumor tissue compared to control lung and decreased upon rapamycin or combination drug treatment. MTORC1 was recently shown to directly

induce lipid biosynthesis (15) therefore decrease in these metabolites may indicate effective inhibition of mTOR by rapamycin.

Treatment with either BIBW 2992 or rapamycin tended to reverse the metabolic shifts observed during tumor induction in lung tissue; however, rapamycin (or the combination) caused a more dramatic reversal for the vast majority of metabolites than BIBW 2992 alone (Fig. 3A). The majority of metabolomic alterations were in pathways affected downstream of mTOR, for example amino acid synthesis. Individual amino acid pathway metabolites significantly altered in lung tumors as compared to control lung were plotted as Z-scores (Fig. 3B) to examine specific effects of the individual versus the combination treatments. The overall pattern of response is similar in all three treatment regimens, not unexpected as both drugs target nodes in the EGFR signaling pathway. Notably, citrate, an intermediate in the TCA cycle, is significantly increased in BIBW 2992 and BIBW 2992 + rapamycin combination-treated lung tumors but not by rapamycin alone. As citrate is also an intermediate in fatty acid and phospholipid synthesis, it is possible that the general decrease in lipids upon drug treatment correlates to less diversion of citrate from the TCA cycle to membrane biosynthetic processes.

Thus this lung cancer model reflects the abnormal metabolism expected in cancer cells, including aberrant nutrient uptake and increased macromolecular synthesis. Moreover, treatment with drugs targeting the EGFR signaling pathway results in reversal of these effects, highlighting the importance of identifying specific metabolites involved in the response.

Key metabolite signature observed in blood and tissue samples during lung tumorigenesis and treatment

In addition to lung tissue, we sampled blood from tumor-bearing animals to determine whether there were metabolic changes that could be used as potential biomarkers indicating the presence of a tumor. Blood was sampled from E-R+ and E+R+ mice at 2 weeks and at terminal stages pi for metabolic profiling. The unbiased screen recovered 26 metabolites with statistical significance of $p \leq 0.05$. The changes after 2 weeks were more profound, possibly due to wasting at the terminal stages. Relative fold-changes were much lower in blood than tissue, most likely due to the dilution of organ-specific effects by the entire blood volume as well as the homeostatic mechanism, which changes or removes many compounds as they enter the bloodstream. Therefore, we performed a validation study with a larger cohort size and compared blood markers from 15 control mice with 15 E+R+ mice at 2 weeks post-induction. Overall, the relative levels of biochemicals that were identified in blood samples from the first study exhibited similar trends to levels measured in samples collected for the validation study. We identified 11 metabolites from both studies that were significantly changed in blood as well as in the induced lung tissue (Table 1).

Evidence of elevated amino acid pools observed in lung were reflected in blood. The branched-chain amino acid conjugates propionyl-carnitine and deoxycarnitine were significantly increased in E+R+ blood and lung tissue compared to control E-R+. These intermediates of valine, leucine, and isoleucine catabolism are indicative of oxidative stress or a shortage of coenzyme A and can build up when the pathway proceeds at rates in excess of downstream capacity to use metabolites in the TCA cycle. The amino acids glutamine, threonine, serine, arginine, and tryptophan were also increased (Table 1), suggestive of increased amino acid synthesis or enhanced protein turnover due to muscle wasting during cancer development. Unlike the other amino acids, aspartate was upregulated in lung and downregulated in blood. Using LC-MS/MS quantification, we verified that glutamine, tryptophan, and arginine were elevated in E+R+ blood and tumors compared to E-R+ control samples induced for 2 weeks, while aspartate was upregulated in lung only (Table 1;

MS targeted assay). In addition, we detected the levels of these amino acids in induced, tumor-bearing lungs after 2 weeks of BIBW 2992, rapamycin, or combination drug treatment (Supplementary Fig. S5). As expected, drug treatment reversed the higher levels of the metabolites observed in the vehicle-treated tumors, though in some cases (aspartate, glutamate) the combination treatment did not decrease the levels beyond the individual treatments. This could be due to the natural variation in a smaller number of samples, or a difference in the 2 week treatment compared to the original analysis after 4 weeks of treatment. The amino acids identified are members of key pathways affected in the treatment response (see below) underscoring the potential significance of small changes in their relative quantities.

Integration of metabolite and gene expression data highlights pathways essential to drug response

While the examination of gene expression or metabolic signatures was informative, we speculated that combining the datasets could reveal the most significant changes. To test this, we performed pathway enrichment analysis on metabolic and transcriptomic signatures. Gene expression and metabolite data from control E+R− mice, induced E+R+ mice and mice treated with the drug combination were mapped together onto KEGG pathways (Supplementary Fig. S6). Each dataset alone did not show significant enrichment in most pathways, but merging the two datasets points to key pathways in cancer cell energy production such as the pentose phosphate pathway, glutathione metabolism, and glycolysis and gluconeogenesis, that are differentially regulated in untreated versus treated tumors. There were 46 significantly enriched pathways that are upregulated in E+R+ tumors compared to E-R+ and of these, 29 were reversed in direction by drug treatment. Two of the pathways, “alanine, aspartate and glutamate metabolism” and “glycolysis and gluconeogenesis” are also of note as, in a study of gene expression profiles in tumor samples from patients with lung adenocarcinoma, gene sets representing those pathways were enriched in patients with poor outcome (11).

Individual pathway maps are informative to highlight the concordance between the metabolites altered in key energy pathways and changes in expression of the enzymes that control production of individual metabolites. For example, both oxidized (GSSG) and reduced glutathione (GSH), as well as amino acids used to synthesize them, were elevated in tumor development (Fig. 4A). Antioxidant enzymes related to glutathione synthesis and coordinately regulated through antioxidant response elements (AREs) and NRF2 binding such as -GCS, glutathione reductase and glutaredoxin were correspondingly upregulated in tumors (Fig. 4A). The glutathione pathway is involved in protection from oxidative stress, a characteristic of rapidly growing cells, by providing a substrate for neutralization of reactive oxygen species (ROS) (16). ROS production and subsequent oxidative stress have been implicated specifically in carcinogenesis driven by oncogenes such as KRAS (17) and EGFR (18). Alternatively, ROS production can occur due to intratumoral hypoxic conditions, leading to oxidative stress which causes the cells to oxidize GSH to GSSG and results in the activation of glutathione synthesis (19). A hypoxia-related gene signature was overexpressed in E+R+ vs. E-R+ lung (Supplementary Fig. S7). For example, GLUT1, a target of hypoxia-inducible factor HIF-1 and mediator of glucose uptake (20), was upregulated in tumors reflecting hypoxic conditions and correlated to an increase in glycolytic metabolites and other glycolytic enzymes (Fig. 4B). After treatment with the drug combination, oxidized and reduced glutathione as well as the HIF-1 target gene signature were downregulated (Fig. 4B, Supplementary Fig. S7), indicating a decrease in energy needs in the tissue.

Glutamine levels were significantly lowered by BIBW 2992 treatment or BIBW 2992 + rapamycin, but not by rapamycin alone (Fig. 4A). Glutamine is the major nutrient consumed

by cancer cells besides glucose and is a precursor of glutathione as well as a source of TCA cycle intermediates. Glutamine metabolism is increased by C-MYC, and downstream gene targets of C-MYC like the glycolytic enzyme enolase (ENO), are upregulated in tumor versus control samples and reversed in drug-treated samples (Fig. 4B and see below).

Several markers of high glucose mobilization, including glucose-6-phosphate, glucose-1-phosphate, and UDP-N-acetyl-glucosamine, which is an important precursor for protein glycosylation and polysaccharide synthesis, were present in higher levels in E+R+ tumor tissue vs. E-R+ control lungs (Fig. 4B). While glucose itself is lower in tumor tissue, it is not a good indicator of tumor glucose levels as it may simply indicate binding of glucose to dead cells. The phosphorylated products fructose-6-phosphate (F-6-P) and fructose-1,6-bisphosphate (F-1,6-BP) are higher in tumors and phosphofructokinase (PFK), which catalyzes the conversion of F-6-P to F-1,6-BP, is correspondingly upregulated. There was also strong evidence for activation of the pentose phosphate pathway (PPP), which provides precursors for growth as well as the NADPH needed for various anabolic reactions (Fig. 4B). For example, expression of transketolase (TKT), which catalyzes the formation of sedoheptulose as well as the conversion of xylulose-5-phosphate back to F-6-P in the PPP, was oppositely regulated in tumors versus combination-treated lungs.

Of note, pyruvate and lactate, the oxidation product of pyruvate, were higher in tumor tissue, as was lactate dehydrogenase A (LDHA) gene expression. This is consistent with previous observations made in tumor tissue, in which pyruvate is converted to lactate (Warburg effect) avoiding energy-producing oxidative phosphorylation. Pyruvate was lowered only by the combination drug treatment, indicating that full suppression of the pathway may be necessary to inhibit glycolysis.

Oncogenic transcription factor activity may be responsible for downstream alteration of key metabolic pathways

Recent studies have suggested that oncoproteins can directly reprogram tumor cell metabolism, and several oncogenes and tumor suppressors have been linked to the regulation of downstream metabolic processes through transcription factor activity (21). To identify candidate transcription factors downstream of oncogenic EGFR activation in our model, we used GSEA and a library of gene sets containing genes with a cis-regulatory element and conserved DNA motifs, representing known or predicted regulatory elements in promoters and 3′-UTRs (13). This bioinformatic methodology was used to identify overrepresented transcription factor binding sites (TFBS) that were present in the promoters of the genes included in gene expression profiles of tumors from untreated E+R+ mice, and vehicle, BIBW 2992, rapamycin or BIBW 2992 plus rapamycin-treated E+R+ mice. Our analysis revealed a cluster of 12 transcription factors that were significantly enriched (FDR value < 0.05) in EGFR tumors compared with normal lung, for example MYC and SREBP1 (Fig. 5A). In contrast, after the first week of drug treatment, the targets of some of these transcription factors were underrepresented, for example NRF1 and NRF2.

To identify metabolic genes that drive the enrichment for each transcription factor gene set, we ran a leading edge analysis of GSEA results described above. By grouping those leading edge genes (i.e., genes with the highest enrichment scores in EGFR tumors) included in TFBS gene sets that were significantly underrepresented after drug treatments (GABP, NRF1, NRF2, SREBP, ELK1 and C-MYC), we were able to categorize them into metabolic processes. As shown in Fig. 5B, the strongest downregulation of metabolic genes activated in EGFR-TL tumors appeared to be after only 1 week of treatment, particularly in response to the combination of BIBW and rapamycin. Key genes such as HK2 and LDHA (glycolysis), and GPX1 and GSS (glutathione metabolism) were affected. After 4 weeks of treatment, the single drug regimens were unable to repress most of the metabolic genes

included in the analysis. Only the drug combination reduced gene expression levels more consistently, suggesting that transcriptional control of metabolic pathways through C-MYC and SREBP, as well as ELK1, NRF1 and NRF2, depends on both EGFR and mTORC1 signaling.

DISCUSSION

Presently, human clinical trials employing BIBW 2992 (afatinib) and rapamycin combination are ongoing (22, 23). The unbiased profiling approach described here highlights the utility of GEMs in rapidly identifying clinically testable hypotheses that might immediately impact the analysis of these ongoing clinical trials, and the design of subsequent human studies. To that point, we observed that several of the prominent pathways modulated during EGFR-driven tumorigenesis were reversed upon combination drug treatment, revealing possible reasons for increased efficacy.

Due to their controlled genetics and environment, mouse models represent ideal tools for the identification of candidate biomarkers. Recent work comparing the plasma proteome of mouse ovarian cancer models with human ovarian cancer cell lines and tissue samples from patients resulted in promising biomarker candidates (24); another study in a mouse pancreatic cancer model revealed proteins that could discriminate human pancreatic cancer sera from controls (25); and protein signatures have been found that distinguish between different types of lung cancer in the mouse (26). We previously identified metabolomic changes in a mouse model of serous epithelial ovarian cancer that overlapped with findings obtained from tissue of human patients with metastatic ovarian cancer (27, 28). As energy metabolism has long been known to be aberrant in cancer, in this study we conducted metabolomic profiling in the EGFR-TL mouse model to identify biochemical processes that might be perturbed both in tumor development and by drug treatment. By comparing tissue and blood metabolomic changes during tumor progression we identified disease-associated changes. Several of the same metabolites have recently been shown to be altered in human lung cancer tissue and sera from patients with squamous cell carcinoma and small cell lung cancer as well as adenocarcinoma (29), indicating fidelity of the mouse models in mimicking the human condition. Furthermore, they demonstrate that the molecular interactions between the tumor and host may be similar in these two species. Since the dilution factor represented by the movement of a compound from the tumor to blood is large, and at the same time other organs may be acting to clear or modify the compound, the ability to validate the blood markers by correlation to lung tumor tissue metabolites in the mouse model is crucial.

As seen in patients (29), murine lung cancer tissue contained higher levels of most amino acids compared to normal lung tissue, including higher levels of glutamine and tryptophan. It is remarkable that high levels of glutamine are maintained although large amounts of glutamine are consumed in cancer cells through glutamine metabolism. Notably, treatment with BIBW 2992 and the combination of BIBW 2992 and rapamycin downregulated the levels of glutamine in the lung tissue, indicating the potential importance of this key source of energy in maintaining cancer cell growth. This could also offer a clue to the synergistic effects of the drug treatment with rapamycin, as glutamine depletion can cause apoptosis in lung cells by affecting pathways that do not require mTOR activity; instead they are MYC-regulated (30). Glutamine can also maintain the TCA cycle when glucose levels are limiting. Growth factor signaling through the PI3K-Akt-mTOR pathway in EGFR-overexpressing mice may be further activated by higher glutamine levels, resulting in increased protein translation (31).

MTORC1, the target of rapamycin and a key regulator of cell growth and proliferation downstream of oncogenic signaling pathways, including EGFR, has been linked previously to cellular metabolism regulation through the transcriptional control of metabolic genes (32, 33), and other recent studies have also linked metabolism to specific oncogenic signaling pathways (34, 35). In our analysis, relating transcriptional control elements from the gene expression data to metabolic processes revealed functional connections between known oncogenes and metabolite changes in the lung tumors. After the first week of drug treatment, binding sites for several transcription factors enriched in tumor samples were underrepresented, for example NRF1 and NRF2. Both BIBW 2992 and rapamycin treatments result in a decrease in the target genes for NRF2 after 1 week, but after 4 weeks only the dual treatment suppresses expression of those genes. NRF2 is a transcriptional activator of cytoprotective enzymes including those involved in glutathione synthesis, and has increased activation in lung cancer tissue and cell lines (36). Therefore, NRF2 activation of glutathione metabolism may be a previously unappreciated mediator of oncogenesis which is inhibited by the combination drug regimen used here.

It was recently observed that mTORC1 signaling increases flux through the pentose phosphate pathway in some measure through activation of SREBP1 (15). SREBP1 is a transcriptional regulator of genes involved in de novo lipid and sterol biosynthesis and is itself regulated by mTOR (32). Interestingly, although rapamycin alone can inhibit mTOR, the SREBP1 gene target set is underrepresented in rapamycin-treated lungs only after 4 weeks of treatment, and even more significantly in the combination treated samples. Targets of C-MYC, a key transcription factor driver in metabolic processes in cancer, are enriched in E+R+ tumors and underrepresented in rapamycin and combination-treated lungs after 1 or 4 weeks of drug treatment.

In summary, this study combines transcriptional and metabolic analyses of a complex *in vivo* model system to examine temporal responses after drug treatment. Examination of lung tumor progression in EGFR-overexpressing TKI-resistant mice as well as a drug regimen known to result in tumor regression revealed marked changes in gene expression and biochemical pathways during tumor growth that were in many cases reversed when treatment was effective, and were different depending on the specific treatment and duration of treatment. These studies can be used to guide future analyses of drug combinations for human disease with targeted agents aimed at resistance by simultaneous blockade of relevant pathways.

Supplementary Material

Refer to Web version on PubMed Central for supplementary material.

Acknowledgments

We thank Catherine Drennan, Melanie Gordon, SAIC's Laboratory Animal Sciences Program, Small Animal Imaging Program, Pathology/Histotechnology Laboratory, and the Laboratory of Molecular Technology for technical assistance; Dr. Marcelino Bernardo and Dr. Peter Choyke for MRI analysis; Maria L. Rodriguez for assistance with HPLC-MS, Patti Lamb for administrative assistance; and Lionel Feigenbaum for program support.

GRANT SUPPORT This research was supported with federal funds from the National Cancer Institute, Intramural Research Program, National Institutes of Health. The content of this publication does not necessarily reflect the views or policies of the Department of Health and Human Services, nor does the mention of trade names, commercial products, or organizations imply endorsement by the U.S. Government.

REFERENCES

1. American Cancer Society. Cancer facts & figures 2011. American Cancer Society; 2011.

2. Howlader, N.; Noone, AM.; Krapcho, M.; Neyman, N.; Aminou, R.; Waldron, W., et al. [cited 2011 September] SEER Cancer Statistics Review, 1975-2008. Surveillance Epidemiology and End Results. Nov. 2010 [Online]. Available from: http://seer.cancer.gov/csr/1975_2008/
3. Doebele RC, Oton AB, Peled N, Camidge DR, Bunn PA Jr. New strategies to overcome limitations of reversible EGFR tyrosine kinase inhibitor therapy in non-small cell lung cancer. Lung Cancer. 2010; 69:1–12. [PubMed: 20092908]
4. Sharma SV, Bell DW, Settleman J, Haber DA. Epidermal growth factor receptor mutations in lung cancer. Nat Rev Cancer. 2007; 7:169–81. [PubMed: 17318210]
5. Mani KM, Lefebvre C, Wang K, Lim WK, Basso K, Dalla-Favera R, et al. A systems biology approach to prediction of oncogenes and molecular perturbation targets in B-cell lymphomas. Mol Syst Biol. 2008; 4:169. Epub 2008 Feb 12. [PubMed: 18277385]
6. Politi K, Pao W. How genetically engineered mouse tumor models provide insights into human cancers. J Clin Oncol. 2011; 29:2273–81. [PubMed: 21263096]
7. Li D, Shimamura T, Ji H, Chen L, Haringsma HJ, McNamara K, et al. Bronchial and peripheral murine lung carcinomas induced by T790M-L858R mutant EGFR respond to HKI-272 and rapamycin combination therapy. Cancer Cell. 2007; 12:81–93. [PubMed: 17613438]
8. Regales L, Balak MN, Gong Y, Politi K, Sawai A, Le C, et al. Development of new mouse lung tumor models expressing EGFR T790M mutants associated with clinical resistance to kinase inhibitors. PLoS One. 2007; 2:e810. [PubMed: 17726540]
9. Li D, Ambrogio L, Shimamura T, Kubo S, Takahashi M, Chirieac LR, et al. BIBW2992, an irreversible EGFR/HER2 inhibitor highly effective in preclinical lung cancer models. Oncogene. 2008; 27:4702–11. [PubMed: 18408761]
10. Barbie DA, Tamayo P, Boehm JS, Kim SY, Moody SE, Dunn IF, et al. Systematic RNA interference reveals that oncogenic KRAS-driven cancers require TBK1. Nature. 2009; 462:108–12. [PubMed: 19847166]
11. Subramanian A, Tamayo P, Mootha VK, Mukherjee S, Ebert BL, Gillette MA, et al. Gene set enrichment analysis: a knowledge-based approach for interpreting genome-wide expression profiles. Proc Natl Acad Sci USA. 2005; 102:15545–50. [PubMed: 16199517]
12. MsSigDB. [cited 2011 September] Molecular Signatures Database v3.0. GSEA. Sep 9. 2010 [Online]. Available from:http://www.broadinstitute.org/gsea/msigdb/index.jsp
13. Xie X, Lu J, Kulbokas EJ, Golub TR, Mootha V, Lindblad-Toh K, et al. Systematic discovery of regulatory motifs in human promoters and 3′ UTRs by comparison of several mammals. Nature. 2005; 434:338–45. [PubMed: 15735639]
14. Hou J, Aerts J, den Hamer B, van Ijcken W, den Bakker M, Riegman P, et al. Gene expression-based classification of non-small cell lung carcinomas and survival prediction. PLoS One. 2010; 5:e10312. [PubMed: 20421987]
15. Duvel K, Yecies JL, Menon S, Raman P, Lipovsky AI, Souza AL, et al. Activation of a metabolic gene regulatory network downstream of mTOR complex 1. Mol Cell. 2010; 39:171–83. [PubMed: 20670887]
16. Estrela JM, Ortega A, Obrador E. Glutathione in cancer biology and therapy. Crit Rev Clin Lab Sci. 2006; 43:143–81. [PubMed: 16517421]
17. Irani K, Xia Y, Zweier JL, Sollott SJ, Der CJ, Fearon ER, et al. Mitogenic signaling mediated by oxidants in Ras-transformed fibroblasts. Science (New York, NY). 1997; 275:1649–52.
18. Nitta M, Kozono D, Kennedy R, Stommel J, Ng K, Zinn PO, et al. Targeting EGFR induced oxidative stress by PARP1 inhibition in glioblastoma therapy. PLoS One. 2010; 5:e10767. [PubMed: 20532243]
19. Franco R, Schoneveld OJ, Pappa A, Panayiotidis MI. The central role of glutathione in the pathophysiology of human diseases. Arch Physiol Biochem. 2007; 113:234–58. [PubMed: 18158646]
20. Furuta E, Okuda H, Kobayashi A, Watabe K. Metabolic genes in cancer: their roles in tumor progression and clinical implications. Biochim Biophys Acta. 2010; 1805:141–52. [PubMed: 20122995]

21. Wise DR, DeBerardinis RJ, Mancuso A, Sayed N, Zhang XY, Pfeiffer HK, et al. Myc regulates a transcriptional program that stimulates mitochondrial glutaminolysis and leads to glutamine addiction. Proc Natl Acad Sci USA. 2008; 105:18782–7. [PubMed: 19033189]
22. Pfizer Clinical Trial Disclosure Group. [cited 2011 September 6] Study Evaluating Neratinib In Combination With Temsirolimus In Subjects With Solid Tumors. ClinicalTrials.gov. Aug 12. 2011 [Online]. Available from: http://www.clinicaltrials.gov/ct2/show/NCT00838539 NLM Identifier: NCT00838539
23. Boehringer Ingelheim Pharmaceuticals. [cited 2011 September 6] Trial of Continuous Once Daily Oral Treatment Using BIBW 2992 (Afatinib) Plus Sirolimus (Rapamune®) in Patients With Non-small Cell Lung Cancer Harbouring an EGFR Mutation and/or Disease Progression Following Prior Erlotinib (Tarceva®). ClinicalTrials.gov. Aug 23. 2011 [Online]. Available from: http://www.clinicaltrials.gov/ct2/show/NCT00993499 NLM Identifier: NCT00993499
24. Pitteri SJ, JeBailey L, Faca VM, Thorpe JD, Silva MA, Ireton RC, et al. Integrated proteomic analysis of human cancer cells and plasma from tumor bearing mice for ovarian cancer biomarker discovery. PLoS One. 2009; 4:e7916. [PubMed: 19936259]
25. Faca VM, Song KS, Wang H, Zhang Q, Krasnoselsky AL, Newcomb LF, et al. A mouse to human search for plasma proteome changes associated with pancreatic tumor development. PLoS Medicine. 2008; 5:e123. [PubMed: 18547137]
26. Taguchi A, Politi K, Pitteri SJ, Lockwood WW, Faca VM, Kelly-Spratt K, et al. Lung cancer signatures in plasma based on proteome profiling of mouse tumor models. Cancer Cell. 2011; 20:289–99. doi: 10.1016/j.ccr.2011.08.007. [PubMed: 21907921]
27. Fong MY, McDunn J, Kakar SS. Identification of metabolites in the normal ovary and their transformation in primary and metastatic ovarian cancer. PLoS One. 2011; 6:e19963. [PubMed: 21625518]
28. Szabova L, Yin C, Bupp S, Guerin TM, Schlomer JJ, Householder DB, Baran ML, Yi M, Song Y, Sun W, McDunn JE, Martin PL, Van Dyke T, Difilippantonio S. Perturbation of Rb, p53, and Brca1 or Brca2 cooperate in inducing metastatic serous epithelial ovarian cancer. Cancer Res. 2012; 72:4141–53. [PubMed: 22617326]
29. Hori S, Nishiumi S, Kobayashi K, Shinohara M, Hatakeyama Y, Kotani Y, et al. A metabolomic approach to lung cancer. Lung Cancer. 2011; 74:284–92. [PubMed: 21411176]
30. Yuneva M, Zamboni N, Oefner P, Sachidanandam R, Lazebnik Y. Deficiency in glutamine but not glucose induces MYC-dependent apoptosis in human cells. J Cell Biol. 2007; 178:93–105. [PubMed: 17606868]
31. Wise DR, Thompson CB. Glutamine addiction: a new therapeutic target in cancer. Trends Biochem Sci. 2010; 35:427–33. [PubMed: 20570523]
32. Porstmann T, Santos CR, Griffiths B, Cully M, Wu M, Leevers S, et al. SREBP activity is regulated by mTORC1 and contributes to Akt-dependent cell growth. Cell Metabolism. 2008; 8:224–36. [PubMed: 18762023]
33. Zoncu R, Efeyan A, Sabatini DM. mTOR: from growth signal integration to cancer, diabetes and ageing. Nat Rev Mol Cell Biol. 2011; 12:21–35. [PubMed: 21157483]
34. Levine AJ, Puzio-Kuter AM. The control of the metabolic switch in cancers by oncogenes and tumor suppressor genes. Science. 2010; 330:1340–4. [PubMed: 21127244]
35. Vander Heiden MG, Cantley LC, Thompson CB. Understanding the Warburg effect: the metabolic requirements of cell proliferation. Science. 2009; 324:1029–33. [PubMed: 19460998]
36. Ohta T, Iijima K, Miyamoto M, Nakahara I, Tanaka H, Ohtsuji M, et al. Loss of Keap1 function activates Nrf2 and provides advantages for lung cancer cell growth. Cancer Res. 2008; 68:1303–9. [PubMed: 18316592]

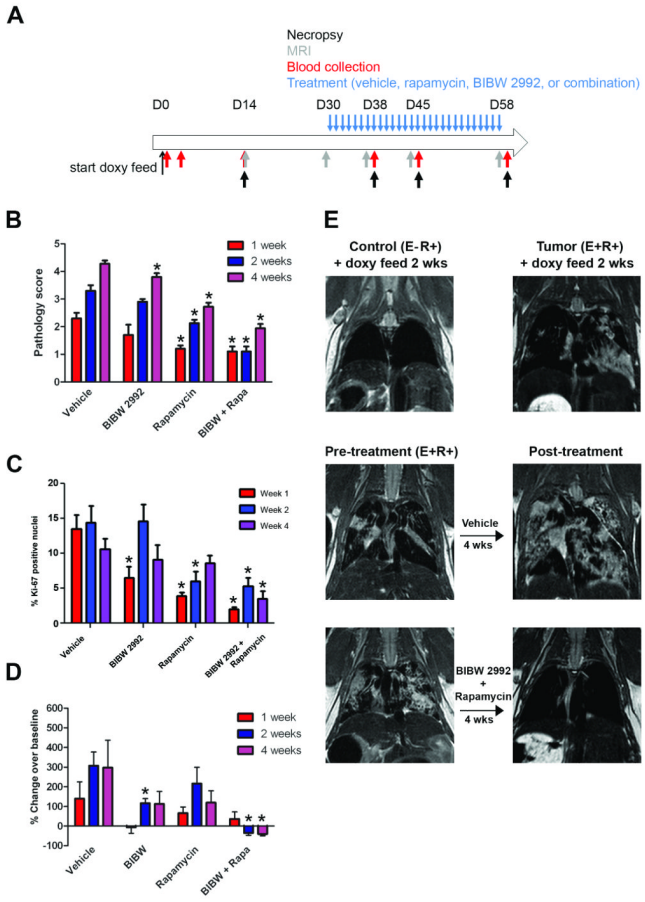

Fig. 1. Quantification of tumor progression in CCSP-rtTA; EGFR-L858R-T790M mice and response to treatment with BIBW 2992 and/or rapamycin

(**A**) Schematic of dosing regimen, blood sampling and imaging for the tumor progression and treatment study. Note that necropsies prior to the treatment start date are for the tumor progression component only. Blood collection for the treatment study was 24 hr post-last dose. (**B**) Histopathological scoring on H&E stained lung tumor samples from treated mice. The average score is plotted for each treatment after 1, 2, or 4 weeks of treatment. (**C**) Automated Ki-67 quantification of vehicle vs. drug-treated lungs at 1, 2 and 4 weeks. The percentage of Ki-67 positive nuclei was quantified using the Ariol Scanning System for the most severely affected lung lobe. 30,000-120,000 cells per lobe were counted. (**D**) MRI quantification was performed as described in the Methods. Each bar represents the percent change of post-treatment vs. baseline lung scan intensity. (B-D) The asterisk indicates $p < 0.05$ compared to the average change in vehicle-treated lungs. Error bars represent standard error of the means. (**E**) Examples of MRI scans of lungs from doxycycline-induced control mice as well as baseline and post-treatment MRI for vehicle-treated and combination BIBW 2992 + rapamycin-treated mice. “Pre-treatment” corresponds to 3 weeks of induction time and “post-treatment” to 4 weeks of treatment time pi. White areas indicate tumor obstruction of the airways, which increases over time in vehicle-treated mice.

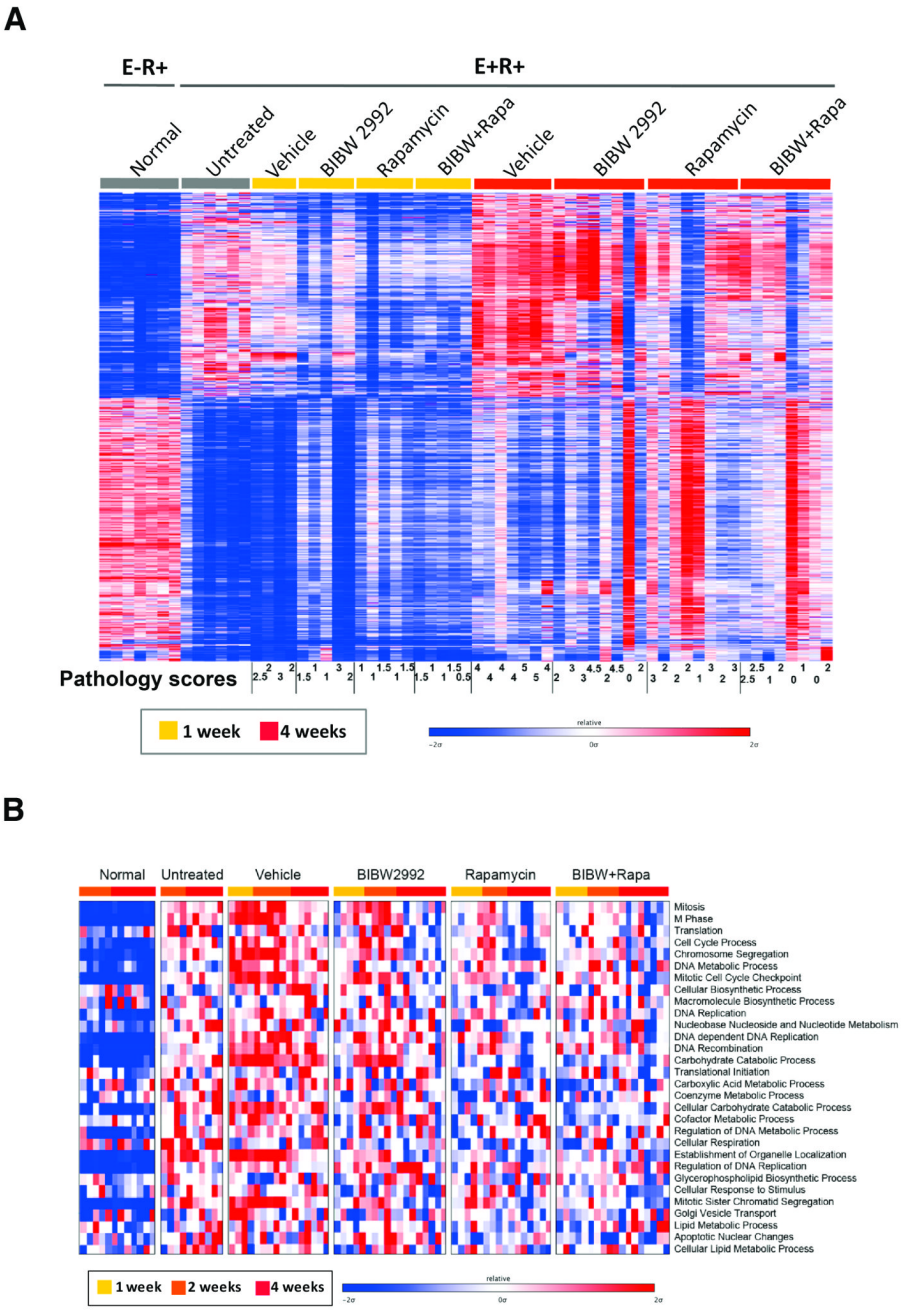

Fig. 2. Supervised clustering shows correlation between tumor status, treatment, and pathology score and pathways

(**A**) Gene expression profiles of normal lung, lung tumors (2 and 4 weeks pi) from untreated EGFR-TL mice, and vehicle, BIBW 2992, rapamycin or BIBW 2992 plus rapamycin treated mice at indicated time points. At the bottom of the heat map are the corresponding pathology scores for each lung sample. (**B**) Single sample gene set enrichment analysis (ssGSEA) scores of samples from (A). A positive enrichment score (in red) indicates a positive correlation between genes in the gene set and the tumor sample expression profile; a negative enrichment score (in blue) indicates the reverse (see also Materials and Methods).

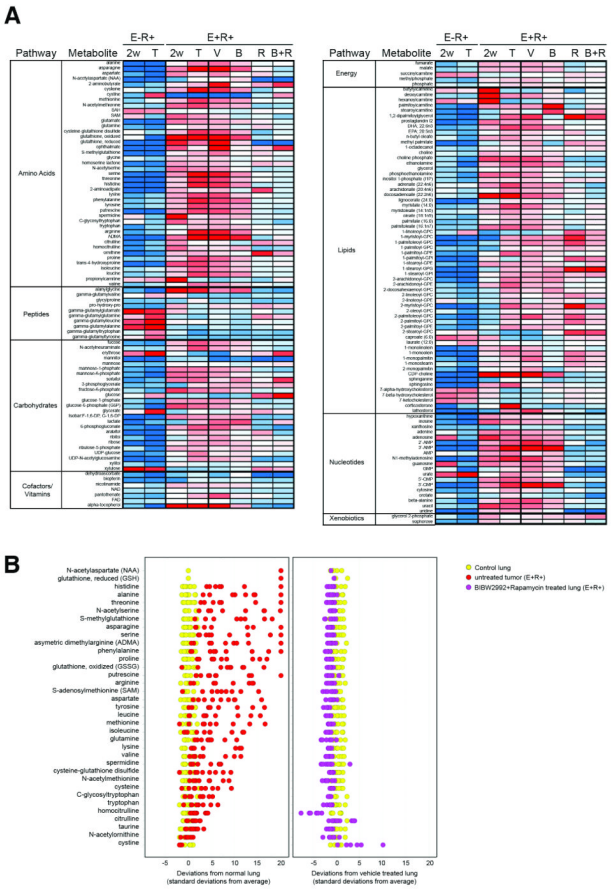

Fig. 3. Widespread metabolomic alterations consistent with tumor development are found within two weeks of induction of the EGFR transgene and are reversed upon treatment

(**A**) Metabolite group means in lung tissue from control (E-R+: 2 weeks (2w) and terminal (T)), tumored untreated (E+R+: 2 weeks (2w) and terminal (T)) as well as tumored treated mice (E+R+: vehicle-treated (V) and BIBW 2992 (B), rapamycin (R), or BIBW 2992 + rapamycin-treated (B+R)). The heat map colors display each group mean level relative to the median for that compound, such that white represents the median, saturated red represents a two-fold increase relative to the median, and saturated blue is one-half the median value. (**B**) Z-score plot of amino acid pathway only, from (A). Each point represents one metabolite in one sample, expressed as the number of standard deviations from the mean of the CONTROL group for that comparison and colored by type (left panel: control E-R+ lung, yellow; tumored E+R+ lung, red; right panel: vehicle-treated lung tumors, yellow, BIBW 2992 + rapamycin-treated tumors, pink). For clarity, the plot was truncated at 20 standard deviations above the mean of the control and vehicle-treated samples, respectively.

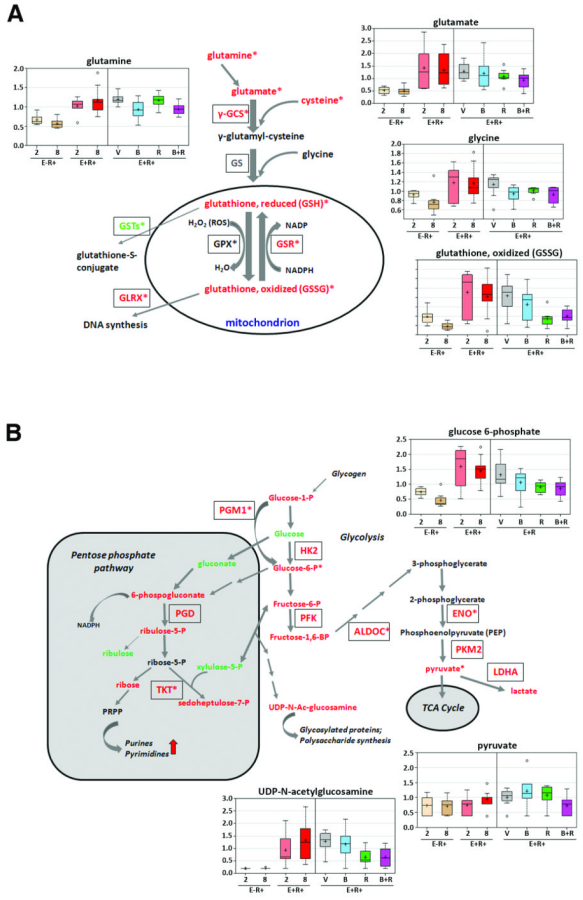

Fig. 4. Metabolic pathway maps highlight correlation between changes in gene expression and metabolite levels

Metabolites and genes that are upregulated in induced E+R+ lung tissue vs. induced E-R+ tissue are shown in red (genes are outlined). Metabolites and genes that are downregulated in E+R+ mice are shown in green. An asterisk indicates that the molecule is regulated in the opposite direction in lungs treated with the BIBW 2992 + rapamycin combination. Box plots represent results for individual metabolites. The Y-axis is a scaled intensity value that represents the ratio between E-R+ and E+R+ lungs at 2 and 8 weeks pi with doxycycline, or on the right side of the plots, the ratio between vehicle-treated (V) and BIBW 2992 (B), rapamycin (R), or BIBW 2992 + rapamycin (B+R)-treated lung samples after 4 weeks of treatment. The + inside box represents mean value, bar inside b represents median value, the upper bar represents maximum of distribution, the lower bar represents minimum of distribution, and the circles represent extreme data points. **(A)** Glutathione metabolism. GPX is unchanged in E+R+ vs. E-R+ lungs but is downregulated in treated lungs. γ–GCS: gamma-glutamylcysteine synthetase; GS: glutathione synthetase; GSR: glutathione reductase; GPX: glutathione peroxidase; GLRX: glutaredoxin; GST: glutathione S-transferase; ROS: reactive oxygen species. **(B)** Glycolysis and pentose phosphate pathways. HK2: Hexokinase 2; PFK phosphofructokinase; LDHA: lactate dehydrogenase; ENO: enolase 1; ALDOC: aldolase C; PKM2: pyruvate kinase M; PGM1: phosphoglucomutase; PGD: phosphogluconate dehydrogenase; TKT: transketolase.

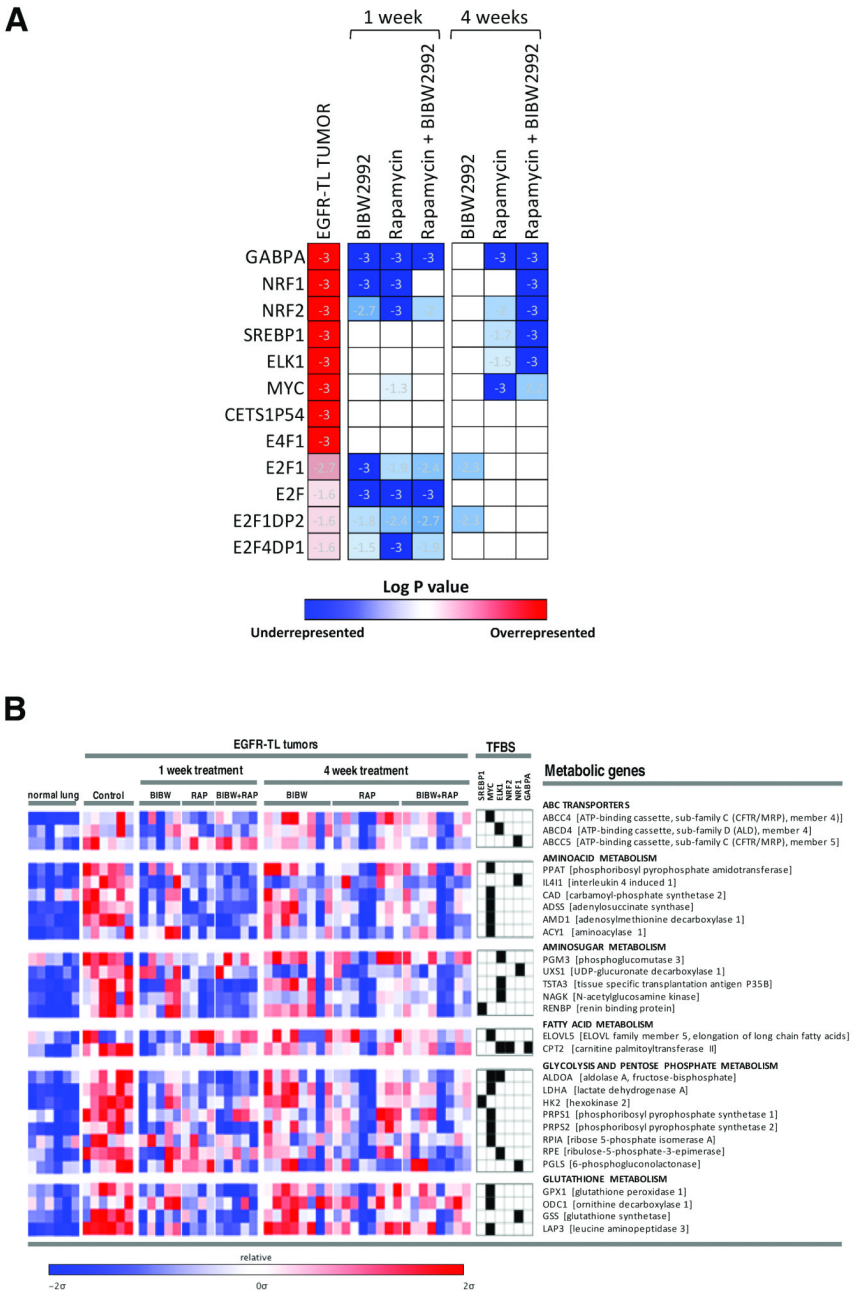

Fig. 5. Oncogenic transcription factor activity is linked to downstream alteration of key metabolic pathways

(**A**) Gene set enrichment analysis of transcription factor-binding sites (TFBS) in expression profiles from normal lung, lung tumors from untreated EGFR-TL mice, and vehicle, BIBW 2992, rapamycin or BIBW 2992 plus rapamycin treated EGFR-TL mice. Heat map shows significant enrichments of TFBS across indicated comparisons. Color scale depicts the logarithm of P value (red, overrepresentation; blue, underrepresentation). (**B**) Leading edge analysis of metabolic genes that have TFBS in their promoters, in normal lung, lung tumors from untreated, and vehicle, BIBW 2992, rapamycin or BIBW 2992 plus rapamycin treated EGFR-TL mice. Heat map shows relative expression levels of genes annotated to KEGG

metabolic pathways across sample set. Black boxes (middle panel) represent the presence of an indicated TFBS in the promoters.

Table 1

Metabolite changes detectable in blood and lung tissue 2 weeks post-induction

Sub Pathway	Metabolite	E+R+/E−R+ Blood (exp1)[1]	E+R+/E−R+ Blood (exp2)[2]	E+R+/E−R+ Lung (exp1)	E+R+/E−R+ Blood (exp2)	E+R+/E−R+ Lung (exp2)
Alanine and aspartate metabolism	aspartate	**0.75** (p=0.0036)	**0.71 (p=0.0054)**	2.13 (p=0.0551)	**0.59** (p=0.0086)	**2.2** (p=0.0018)
Glutamate metabolism	glutamine	**1.14** (p=0.0012)	1.32 (p=0.0709)	**1.52** (p=0.0147)	**1.58** (p<0.001)	**1.7** (p=0.0368)
Glycine, serine and threonine metabolism	threonine	**1.55** (p<0.001)	**1.57** (p=0.0148)	**2.50** (p=0.0252)	n.d.[3]	n.d.
Glycine, serine and threonine metabolism	serine	**1.35** (p=0.0437)	**1.36** (p=0.0006)	**2.60** (p=0.0359)	n.d.	n.d.
Tryptophan metabolism	tryptophan	**1.40** (p<0.001)	**1.45** (p=0.0086)	**3.31** (p=0.0099)	**1.80** (p=0002)	**2.0** (p=0.0344)
Tryptophan metabolism	3-indoxyl sulfate	**1.51** (p=0.0254)	**1.47** (p=0.0309)	**1.62** (p=0.0078)	n.d.	n.d.
Urea cycle; arginine-, proline-, metabolism	arginine	**1.29** (p=0.0062)	**1.40** (p=0.0254)	1.44 (p=0.2250)	**1.45** (p=0.0014)	**3.3** (p=0.0004)
Carnitine metabolism	deoxycarnitine	**1.25** (p<0.001)	**1.26** (p=0.0057)	1.68 (p=0.0857)	n.d.	n.d.
Carnitine metabolism	propionylcarnitine	**1.26** (p<0.001)	**1.39** (p=0.0032)	**2.39** (p=0.0148)	n.d.	n.d.
Lysolipid	1-arachidoylglycerophosphocholine	**0.28** (p=0.0037)	**0.34** (p=0.0406)	n.d.	n.d.	n.d.
Sterol/Steroid	corticosterone	**2.41** (p<0.001)	1.24 (p=0.2535)	**2.67** (p=0.0108)	n.d.	n.d.
		Metabolon Platform			**MS targeted assay**	

[1] exp1: experiment 1, n = 8 E−R+, 8 E+R+ mice

[2] exp2: experiment 2, n = 15 E−R+, 15 E+R+ mice

[3] n.d.: not done